Chen *et al.*
Chinese Journal of Mechanical Engineering (2022) 35:71
https://doi.org/10.1186/s10033-022-00748-7

Chinese Journal of Mechanical Engineering

ORIGINAL ARTICLE

Open Access

Lane-Exchanging Driving Strategy for Autonomous Vehicle via Trajectory Prediction and Model Predictive Control

Yimin Chen[1,3], Huilong Yu[2*], Jinwei Zhang[3] and Dongpu Cao[4]

Abstract

The cooperation between an autonomous vehicle and a nearby vehicle is critical to ensure driving safety in the lane-exchanging scenario. The nearby vehicle trajectory needs to be predicted, from which the autonomous vehicle is controlled to prevent possible collisions. This paper proposes a lane-exchanging driving strategy for the autonomous vehicle to cooperate with the nearby vehicle by integrating vehicle trajectory prediction and motion control. A trajectory prediction method is developed to anticipate the nearby vehicle trajectory. The Gaussian mixture model (GMM), together with the vehicle kinematic model, are synthesized to predict the nearby vehicle trajectory. A potential-field-based model predictive control (MPC) approach is utilized by the autonomous vehicle to conduct the lane-exchanging maneuver. The potential field of the nearby vehicle is considered in the controller design for collision avoidance. On-road driving data verification shows that the nearby vehicle trajectory can be predicted by the proposed method. CarSim® simulations validate that the autonomous vehicle can perform the lane-exchanging maneuver and avoid the nearby vehicle using the proposed driving strategy. The autonomous vehicle can thus safely perform the lane-exchanging maneuver and avoid the nearby vehicle.

Keywords: Autonomous vehicle, Lane-exchanging, Vehicle trajectory prediction, Potential field, Model predictive control

1 Introduction

The autonomous vehicle is a promising technique that draws great attention from automotive manufactures, research institutes, and high-tech companies recently [1], owing to its great potential of improving driving safety and traffic efficiency [2, 3]. However, the complex driving scenarios impede the development and application of the automated driving technology [4]. With the appearance of nearby road users, the autonomous vehicle has to cooperate with other traffic participants to ensure the road safety and efficiency [5].

The trajectory prediction of nearby vehicles have been investigated to enable the autonomous vehicle to collaborate with other road users. A unified framework is proposed for the maneuver classification and the motion prediction of surrounding vehicles [6]. After learning the probability distribution from the previous motion patterns, the vehicle trajectory can be anticipated by calculating the probability of the future motion [7]. The constant yaw rate and acceleration model and the maneuver recognition model are combined to predict vehicle trajectory [8]. Similarly, the physical-based method and the maneuver-based method are integrated to predict the vehicle trajectory via an interactive multiple model [9]. The recurrent neural network and the 3D trajectory cues are utilized to anticipate the surrounding vehicle trajectories [10]. The driver behaviors are anticipated through the input-output hidden Markov model for cooperating

*Correspondence: huilong.yu@bit.edu.cn

[2] School of Mechanical Engineering, Beijing Institute of Technology, Beijing 100081, China
Full list of author information is available at the end of the article

Springer Open

© The Author(s) 2022. **Open Access** This article is licensed under a Creative Commons Attribution 4.0 International License, which permits use, sharing, adaptation, distribution and reproduction in any medium or format, as long as you give appropriate credit to the original author(s) and the source, provide a link to the Creative Commons licence, and indicate if changes were made. The images or other third party material in this article are included in the article's Creative Commons licence, unless indicated otherwise in a credit line to the material. If material is not included in the article's Creative Commons licence and your intended use is not permitted by statutory regulation or exceeds the permitted use, you will need to obtain permission directly from the copyright holder. To view a copy of this licence, visit http://creativecommons.org/licenses/by/4.0/.

with the nearby vehicles [11]. The deep recurrent neural networks are used to develop an integrated time series model for estimating the drivers' brake intention [12]. The drivers' driving styles and the road environments are considered to develop a curve speed model [13]. The drivers' intention and maneuver are recognized by the inductive multilabel classification, in order to assist the drivers in the shared control scheme [14]. The drivers' visual scanning behaviors at both the signalized and the unsignalized intersections are investigated to improve the road safety [15]. With the predicted trajectories of the surrounding vehicles, the motion control methods are developed to manipulate the autonomous vehicle accordingly via understanding the behaviors of the nearby vehicles. The robust control, back-stepping control, MPC and many other approaches are utilized in vehicle motion controller design. The robust control method is used to design the trajectory tracking controllers considering the modeling errors and the system uncertainties [16]. The control efforts are computed by solving a set of linear matrix inequalities [17]. A trajectory tracking controller using the back-stepping method is designed to track the planned trajectory and velocity in different T-intersection driving scenarios [18]. The MPC algorithm is employed for the vehicle motion control, considering its advantages of dealing with the system constraints [19]. By converting the path-tracking control into the yaw stabilization problem, the vehicle motion control is achieved by the integral sliding mode control method [20]. An optimal control approach is proposed to control the 4-independent wheel driving electric vehicles by solving a large-scale nonlinear optimization problem [21]. The nonlinear decoupling method is used to improve the maneuverability and stability of electric vehicles [22]. The steering characteristics of an individual driver are considered to design the motion controller of the electric vehicles [23]. With the consideration of driver behaviors, the intelligent vehicles can cooperate with human drivers in different driving scenarios.

The lane-exchanging is one of the most challenging driving scenarios. The ground vehicles may need to perform the lane-exchanging maneuvers in the road fork driving situation. Under this driving condition, the nearby vehicle intends to change to the right-lane where the autonomous vehicle drivers, at the same time, the autonomous vehicle needs to switch to the left-lane and yield to the nearby vehicle, as shown in Figure 1. Some research efforts have been devoted to the studies of lane-exchanging scenario. The driver characteristics are considered in trajectory planning for the two vehicles to switch lane simultaneously [24]. The transportation requests can be exchanged to facilitate the vehicle collaboration in the lane-exchanging scenario [25]. Despites

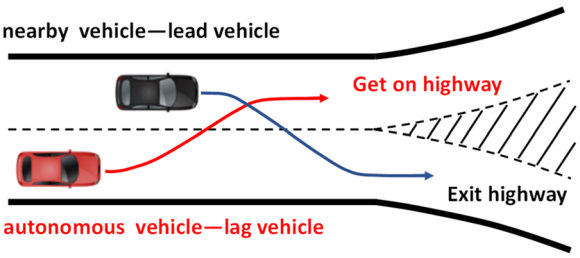

Figure 1 Lane-exchanging scenario

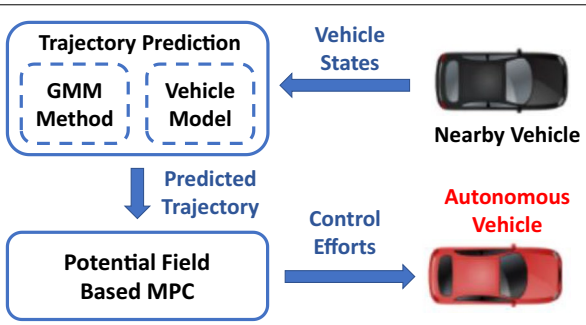

Figure 2 Structure of the lane-exchanging driving strategy

the research efforts above, the lane-exchange driving strategies of the autonomous vehicles are limited. Since the nearby vehicle trajectory is commonly assumed to be known in most studies, it is challenging to consider the nearby vehicle trajectory in the driving strategy design. To overcome these limitations, it is crucial to understand the nearby vehicle trajectory so that the autonomous vehicle can be controlled accordingly for inter-vehicle cooperation and collision avoidance.

This paper proposes a lane-exchanging driving strategy by synthesizing the trajectory prediction and the potential-field-based MPC. The autonomous vehicle should yield to the nearby vehicle that is driven by a human driver. In this study, the nearby vehicle is the lead-vehicle, whereas the autonomous vehicle is the lag-vehicle. The effects of the autonomous vehicle on the nearby vehicle are assumed to be small in the lead-lag condition. The trajectory of the nearby vehicle is predicted to facilitate the cooperation between the two vehicles. The structure of the proposed method is depicted in Figure 2.

As shown in Figure 2, the nearby vehicle trajectory is predicted for the motion control of the autonomous vehicle. A trajectory prediction method is developed by combining the long-term trajectory prediction and short-term trajectory prediction. The GMM method is employed to predict the vehicle trajectory in the long-term, meanwhile, the vehicle kinematic model is used to anticipate that in the short-term. The predicted trajectory

is sent to the motion control of the autonomous vehicle through the potential-field-based MPC method. Considering the potential fields of the nearby vehicle, the control efforts are computed to change the lane and avoid possible collisions in the lane-exchanging scenario. The contributions of this paper are listed as follows.

(1) A lane-exchanging driving strategy integrating vehicle trajectory prediction and motion control is developed. The predicted trajectories of the nearby vehicle are considered and integrated in the motion control of the autonomous vehicle, which facilitates the inter-vehicle cooperation.
(2) A trajectory prediction method is formed to anticipate the nearby vehicle trajectory. The long-term trajectory prediction using the GMM and the short-term trajectory prediction using the vehicle kinematic model are combined to anticipate the vehicle trajectory.
(3) The potential-field-based MPC method is utilized to perform the lane-exchanging maneuver with the predicted trajectory of the nearby vehicle. To avoid possible collisions, the potential field of the nearby vehicle is constructed through trajectory prediction and included in the controller design.

The structure of this paper is as follows. The trajectory prediction method for anticipating the nearby vehicle trajectory is introduced in Section 2. With the predicted trajectory, the potential-field-based MPC algorithm is detailed in Section 3 to conduct the lane-exchanging maneuver and avoid collision with the nearby vehicle. The simulation results are given in Section 4 and the conclusion is provided in Section 5.

2 Nearby Vehicle Trajectory Prediction

The nearby vehicle trajectory is predicted to facilitate the cooperation between two vehicles in the lane-exchanging scenario. The predicted trajectory of the nearby vehicle is obtained by combing the short-term trajectory predicted through the vehicle kinematic model and the long-term trajectory predicted through the GMM method.

2.1 Vehicle Trajectory Predicted by Vehicle Kinematic Model

The vehicle trajectory in the nearby future mainly depends on vehicle motion. The vehicle kinematic model that illustrates the relationship between vehicle velocity and vehicle position is used to predict the vehicle trajectory in the short-term [8]. The schematic diagram of the vehicle kinematic model is shown in Figure 3.

As shown in Figure 3, for vehicle states at time instance t, the vehicle longitudinal and lateral positions of the center of gravity (CG) are x_t and y_t respectively, v_t is vehicle velocity, ω_t is vehicle yaw rate, a_t is vehicle acceleration, and ψ_t is vehicle yaw angle. To predict the vehicle trajectory in the near future, the vehicle acceleration and yaw rate are assumed to be constant in the prediction horizon, i.e., $a_t = a_0$ and $\omega_t = \omega_0$. The predicted vehicle velocity and yaw angle can thus be expressed as

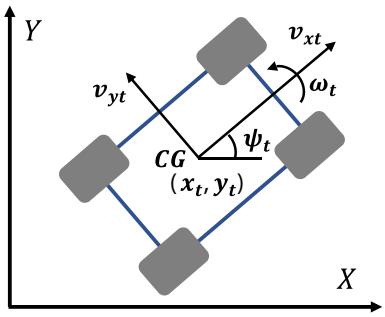

Figure 3 Vehicle kinematic model

$$v_t = a_0 t + v_0, \tag{1}$$

$$\psi_t = \omega_0 t + \psi_0, \tag{2}$$

where a_0 is the initial vehicle acceleration and ω_0 is the initial vehicle yaw rate. v_0 and ψ_0 are vehicle velocity and yaw angle at the initial prediction time, respectively. Since vehicle positions are represented in the Cartesian coordinate, the vehicle velocities in the longitudinal and lateral directions need to be computed. According to vehicle kinematic model, vehicle velocity can be computed as

$$v_{xt} = v_t \cos \psi_t, \tag{3}$$

$$v_{yt} = v_t \sin \psi_t, \tag{4}$$

where v_{xt} and v_{yt} are the vehicle velocity in the longitudinal and the lateral directions at the prediction time t, respectively. Let the initial vehicle longitudinal and lateral positions be x_0 and y_0. Then, the vehicle trajectory at the future time t can be obtained by integrating the velocities v_{xt} and v_{yt} [9], which are

$$x_t = \frac{a_0}{\omega_0^2} \cos \psi_t + \frac{v_t}{\omega_0} \sin \psi_t - \frac{a_0}{\omega_0^2} \cos \psi_0 - \frac{v_0}{\omega_0} \sin \psi_0 + x_0, \tag{5}$$

$$y_t = \frac{a_0}{\omega_0^2} \sin \psi_t - \frac{v_t}{\omega_0} \cos \psi_t - \frac{a_0}{\omega_0^2} \sin \psi_0 + \frac{v_0}{\omega_0} \cos \psi_0 + y_0. \tag{6}$$

The predicted trajectory consists of vehicle longitudinal position x_t and lateral position y_t, which can be written as

$$Tr_1(t) = (x_t, y_t), \tag{7}$$

where $Tr_1(t)$ is the trajectory predicted by the vehicle kinematic model. The constant yaw rate and acceleration model is employed for short-term trajectory prediction via Eqs. (5) and (6).

2.2 Vehicle Trajectory Predicted by GMM

Vehicle trajectory in the long-term relates to the drivers' intention and maneuver. In the lane-exchanging scenario, the nearby vehicle will change to the lane where the autonomous vehicle drives. Therefore, the long-term trajectory of the nearby vehicle can be anticipated by learning the historical driving data of the lane-change maneuver when the drivers' lane-change intention is identified. As this study mainly focuses on the vehicle trajectory prediction, the lane-change intention of the nearby vehicle is assumed to be given or anticipated by other advanced algorithms [26].

For the purpose of predicting vehicle trajectory in the long-term, it is assumed that the future vehicle trajectory depends on the historical vehicle trajectory. Therefore, the probability distribution of the historical trajectory is utilized to infer that of the future trajectory. Considering its advantages of approximating various kinds of the probability distribution, the GMM method is used to represent the probability distribution of vehicle trajectories. The evolution of vehicle trajectory is thus regarded as a Gaussian process, and the Gaussian regression can be adopted for vehicle trajectory prediction. The procedures of vehicle trajectory prediction consist of two stages: the GMM model is firstly obtained by learning the lane-change driving data; then the future vehicle trajectory can be anticipated via the conditional Gaussian distribution, given the historical vehicle trajectory.

In order to obtain a uniform representation of the vehicle trajectory and ensure the path smoothness, the vehicle trajectory is represented by Chebyshev polynomial to facilitate the trajectory prediction [7]. The historical vehicle trajectory can be expressed as

$$Tr_h(t) = \sum_{i=1}^{m} x_{hi} Ch_{hi}(t), \tag{8}$$

where $Tr_h(t)$ is the historical vehicle trajectory. $Ch_{hi}(t)$ is the Chebyshev polynomial of the historical trajectory evaluated at time step t. The subscript i indicates the order of the Chebyshev polynomial and $i = 1, 2, \ldots, m$. x_{hi} is the Chebyshev polynomial coefficient, and the coefficient vector of the historical trajectory is $\boldsymbol{x_h} = [x_{h1} x_{h2} \ldots x_{hm}]^{\mathrm{T}}$. Based on Eq. (8), the historical vehicle trajectory is decomposed as the Chebyshev polynomials and their coefficients. The polynomial coefficients are used to represent the historical vehicle trajectory. Similarly, the future vehicle trajectory can be expressed in the same way. The coefficient vector of the future vehicle trajectory is $\boldsymbol{x}_f = \left[x_{f1} x_{f2} \ldots x_{fm}\right]^{\mathrm{T}}$. Since vehicle trajectory is represented by polynomial coefficients, the vehicle trajectory prediction can be converted into the prediction of the polynomial coefficients.

Owing to the relationship between the historical and future vehicle trajectories, together with the Chebyshev polynomials representation, the future vehicle trajectory is predicted by computing the future polynomial coefficients using the historical polynomial coefficient. The coefficient vector $\boldsymbol{x_h}$ of the historical trajectory is used as the input feature, and the prediction output is the coefficient vector $\boldsymbol{x}_f$ of the future vehicle trajectory. In order to describe the relationship between the history and the future coefficients, a state vector is defined as

$$\boldsymbol{GS} = \begin{bmatrix} \boldsymbol{x}_h \\ \boldsymbol{x}_f \end{bmatrix}. \tag{9}$$

The distribution of the state vector $\boldsymbol{GS}$ is assumed as a Gaussian mixture distribution, which is written as

$$\boldsymbol{GS} \sim \sum_{k=1}^{n} \omega_k \mathbb{N}(\boldsymbol{\mu_k}, \boldsymbol{\Sigma}_k), \tag{10}$$

where $\boldsymbol{u_k}$ and $\boldsymbol{\Sigma_k}$ are the mean and the covariance of the Gaussian component k. ω_k is the weight of the corresponding Gaussian component. n is the number of the Gaussian components, and a single Gaussian component k can be written as

$$\boldsymbol{\mu_k} = \begin{bmatrix} \mu_{k,h} \\ \mu_{k,f} \end{bmatrix}, \tag{11}$$

$$\boldsymbol{\Sigma}_k = \begin{pmatrix} \Sigma_{k,h} & \Sigma_{k,hf} \\ \Sigma_{k,fh} & \Sigma_{k,f} \end{pmatrix}, \tag{12}$$

where the subscript h denotes the history information and the subscript f represents the future information. The mean $\boldsymbol{u_k}$ and covariance $\boldsymbol{\Sigma}_k$ of the component k of the GMM can be obtained by learning the driving dataset. The GMM is utilized to approximate the distribution of the historical and future trajectories.

After inferring the GMM, the state vector $\boldsymbol{GS}$ can be approximated. The relationship between the historical trajectory coefficient and the future trajectory coefficient are described by Gaussian process. Then, the conditional mixture distribution $p(\boldsymbol{x_f}|\boldsymbol{x_h})$ is used to predict the future trajectory coefficient $\boldsymbol{x_f}$, given the history trajectory coefficient $\boldsymbol{x_h}$. As the distribution of the polynomial coefficients consists of n Gaussian components, the covariance

of the Gaussian component k of the conditional mixture distribution is written as

$$\Sigma_{k,f|h} = \Sigma_{k,f} - \Sigma_{k,fh}\Sigma_{k,h}^{-1}\Sigma_{k,hf}. \tag{13}$$

The mean of the Gaussian component k of the conditional mixture distribution can be calculated as

$$\mu_{k,f|h} = \mu_{k,f} + \Sigma_{k,fh}\Sigma_{k,h}^{-1}(\boldsymbol{x_h} - \mu_{k,h}). \tag{14}$$

For the Gaussian components k, the weight of the conditional mixture distribution is computed as

$$\omega_{k|h} = \frac{\omega_k p(\boldsymbol{x_h}|\mu_{k,x_h}, \Sigma_{k,x_h})}{\sum_{k=1}^{n} \omega_k p(\boldsymbol{x_h}|\mu_{k,x_h}, \Sigma_{k,x_h})}. \tag{15}$$

Eqs. (13)–(15) define a full conditional probability density function of the polynomial coefficient of the future trajectory. The conditional mixture distribution $p(\boldsymbol{x}_f|\boldsymbol{x}_h)$ of the future trajectory coefficients can be given as

$$p(\boldsymbol{x_f}|\boldsymbol{x_h}) = \sum_{k=1}^{n} \omega_{k|h}\mathbb{N}(\mu_{k,f|h}, \Sigma_{k,f|h}), \tag{16}$$

From Eq. (16), the conditional mixture distribution of the polynomial coefficients of the future trajectory can be obtained. The mean and covariance of the conditional probability distribution are the combination of the n Gaussian components, which are written as

$$\mu_{\sigma f|h} = \sum_{k=1}^{n} \omega_{k|h}\mu_{k,f|h}, \tag{17}$$

$$\boldsymbol{\Sigma}_{\sigma_f|h} = \sum_{k=1}^{n} \omega_{k|h}(\Sigma_k + (\mu_{k,f|h} - \mu_{\sigma_f|h})(\mu_{k,f|h} - \mu_{\sigma_f|h})^{\mathrm{T}}). \tag{18}$$

The future vehicle trajectory is predicted by computing the distribution of the polynomial coefficients of the future trajectory, which is approximated by the conditional mixture distribution. Since the vehicle trajectory is represented by the Chebyshev polynomial, the future vehicle trajectory can be given as

$$Tr_2(t) = Ch(t) \cdot \boldsymbol{x}_f, \tag{19}$$

where $Tr_2(t)$ is the predicted vehicle trajectory. $\boldsymbol{x}_f$ is the predicted coefficient vector of the Chebyshev polynomial. $Ch(t)$ is the Chebyshev polynomial evaluated at time t. The future vehicle trajectory can be predicted through above procedures.

2.3 Trajectory Prediction Integration

The short-term trajectory prediction and the long-term trajectory prediction are integrated to obtain the final predicted vehicle trajectory. The vehicle kinematic model is accurate in the short-term prediction, meanwhile, the GMM method emphases on the long-term prediction. To obtain the final trajectory prediction, a weighting function is utilized to combine the predicted trajectories in both the short-term and long-term.

Considering the smoothness of vehicle trajectory, the cubic spline function $f(t)$ is used to construct the weighing function that integrates the two predicted trajectories. The weighting function is defined as a cubic spline within the prediction horizon $[\,0,\ T\,]$ and $0 \le f(t) \le 1$. Then, the prediction trajectory can be written as

$$Tr(t) = f(t)Tr_1(t) + (1 - f(t))Tr_2(t). \tag{20}$$

The final predicted trajectory is represented by $Tr(t)$. With the prediction time t increases from 0 to T, the weighting function $f(t)$ is decreasing from 1 to 0. At the beginning of the trajectory prediction, the short-term predicted trajectory $T_{r1}(t)$ dominates the trajectory prediction and the weighting function $f(t)$ is close to 1. As the prediction time increase, the predicted trajectory is close to the long-term predicted trajectory $T_{r2}(t)$ which means the weighting function $f(t)$ approaches to 0.

3 Potential Field Based Model Predictive Control

With the predicted nearby vehicle trajectory, the potential-field-based MPC algorithm is used to perform the lane-exchanging maneuver and cooperate simultaneously with the nearby vehicle.

3.1 Vehicle System Model

A control-oriented vehicle model is formed for the controller design. The bicycle vehicle model that simplifies the model complexity while preserving accuracy is utilized to describe vehicle motion on the ground. The bicycle vehicle model is illustrated in Figure 4.

As shown in Figure 4, the bicycle vehicle model illustrates the vehicle planar motion. The vehicle longitudinal motion, lateral motion and yaw motion are considered, whereas the vehicle pitch motion and roll motion are

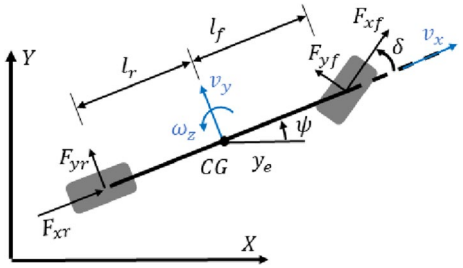

Figure 4 Vehicle dynamic model

ignored. Then, the vehicle motion equations can be written as [27]

$$\begin{cases} \dot{X} = v_x \cos\psi - v_y \sin\psi, \\ \dot{Y} = v_x \sin\psi + v_y \cos\psi, \\ \dot{\psi} = \omega_z, \\ \dot{v}_x = v_y \omega_z + \frac{F_x}{m}, \\ \dot{v}_y = -v_x \omega_z + \frac{F_{yf}+F_{yr}}{m}, \\ \dot{\omega}_z = \frac{F_{yf} l_f - F_{yr} l_r}{I_z}, \end{cases} \tag{21}$$

where X and Y are vehicle global positions in the longitudinal and lateral directions, respectively. F_x is the longitudinal tire force. F_{yf} is the lateral tire force of the front wheels, and F_{yf} is that of the rear wheel. l_f and l_r are the distances from vehicle center of gravity to the front axle and rear axle, respectively. m is the total vehicle mass, and I_z is vehicle yaw moment of inertia. ψ is vehicle yaw angle, and ω_z is vehicle yaw rate, so that the yaw motion of the autonomous vehicle can be considered in the controller design. v_x and v_y are vehicle longitudinal and lateral velocity, respectively.

In the lane-exchanging scenario, the vehicle yaw angle is assumed small [24]. Therefore, we can have the conditions $\cos\psi \approx 1$ and $\sin\psi \approx \psi$. The vehicle global position can then be simplified as

$$\dot{X} = v_x - v_y \psi, \tag{22}$$

$$\dot{Y} = v_x \psi + v_y. \tag{23}$$

Considering the normal driving conditions studied in this paper, the linear tire model is used to compute the lateral tire forces, which are

$$F_{yf} = C_f(\delta - \frac{v_y + l_f \omega_z}{v_x}), \tag{24}$$

$$F_{yf} = -C_r \frac{v_y - l_r \omega_z}{v_x}, \tag{25}$$

where δ is the steering angle of the front wheel. C_f and C_r are the cornering stiffness of the front axle and the rear axle, respectively. By substituting Eqs. (23)–(25) into Eq. (21), the vehicle system model in Eq. (21) can be rewritten into the state space representation, which is

$$\begin{cases} \dot{\boldsymbol{\xi}} = \boldsymbol{A}\boldsymbol{\xi} + \boldsymbol{B}\boldsymbol{u}, \\ \boldsymbol{\eta} = \boldsymbol{C}\boldsymbol{\xi}, \end{cases} \tag{26}$$

where the state vector is $\boldsymbol{\xi}$, and $\boldsymbol{\xi} = \left[X, v_x, Y, v_y, \psi, \omega_z\right]^{\mathrm{T}}$. The system output would be $\boldsymbol{\eta} = [Y, \psi, v_x]^{\mathrm{T}}$. The control inputs are the steering angle and the longitudinal tire force, i.e., $\boldsymbol{u} = [\delta\, F_x]^{\mathrm{T}}$. $\boldsymbol{A}$ is the system matrix, $\boldsymbol{B}$ is the control matrix, and $\boldsymbol{C}$ is the output matrix. The above matrices can be expressed as

$$\boldsymbol{A} = \begin{bmatrix} 0 & 1 & 0 & 0 & -v_y & 0 \\ 0 & 0 & 0 & 0 & 0 & v_y \\ 0 & 0 & 0 & 1 & v_x & 0 \\ 0 & 0 & 0 & -\frac{C_f + C_r}{m v_x} & 0 & \frac{C_r l_r - C_f l_f}{m v_x} - v_x \\ 0 & 0 & 0 & 0 & 0 & 1 \\ 0 & 0 & 0 & \frac{l_r C_r - l_f C_f}{I_z v_x} & 0 & -\frac{l_r^2 C_r + l_f^2 C_f}{I_z v_x} \end{bmatrix},$$

$$\boldsymbol{B} = \begin{bmatrix} 0 & \frac{1}{m} & 0 & 0 & 0 & 0 \\ 0 & 0 & 0 & \frac{C_f}{m} & 0 & \frac{l_f C_f}{m} \end{bmatrix}^{\mathrm{T}},$$

$$\boldsymbol{C} = \begin{bmatrix} 0 & 0 & 1 & 0 & 0 & 0 \\ 0 & 0 & 0 & 0 & 1 & 0 \\ 0 & 1 & 0 & 0 & 0 & 0 \end{bmatrix}. \tag{27}$$

The vehicle model in Eq. (26) is utilized as the predictive model of the MPC algorithm. Under the MPC scheme, the vehicle system is discretized as

$$\begin{cases} \boldsymbol{\xi}(k+1) = \boldsymbol{A_k}\boldsymbol{\xi}(k) + \boldsymbol{B_k}\boldsymbol{u}(k), \\ \boldsymbol{\eta}(k) = \boldsymbol{C_k}\boldsymbol{\xi}(k), \end{cases} \tag{28}$$

where $\boldsymbol{A_k}$ is the discretized system matrix, and $\boldsymbol{A_k} = \boldsymbol{I} + \boldsymbol{T}_s\boldsymbol{A}$. $\boldsymbol{B_k}$ is the discretized control matrix and $\boldsymbol{B_k} = T_s\boldsymbol{B}$. $\boldsymbol{T}_s$ is the sampling time. The discretized output matrix is $\boldsymbol{C_k}$. The incremental of the control efforts is written as $\Delta\boldsymbol{u}(k)$ that satisfies the condition $\Delta\boldsymbol{u}(k) = \boldsymbol{u}(k) - \boldsymbol{u}(k-1)$.

3.2 Potential Fields

The autonomous vehicle has to cooperate with the nearby vehicle for collision avoidance in the lane-exchanging scenario. The nearby vehicle is thus regarded as a moving obstacle that needs to be avoided when the autonomous vehicle changes to the other lane. By predicting the nearby vehicle trajectory, the potential field of the nearby vehicle is constructed and considered in the controller design, in order to avoid possible collisions between the two vehicles. The potential field of the nearby vehicle can be written as [28]

$$U_o(X, Y) = \frac{a}{SD(\frac{\Delta X}{X_s}, \frac{\Delta Y}{Y_s})^b}, \tag{29}$$

where a is the intensity parameter, and b is the shape parameter of the potential field of the nearby vehicle. ΔX and ΔY are the relative distances between two vehicles in the longitudinal and the lateral directions, respectively. The term $SD(\bullet)$ represents the signed distance that represents the relative position between the two vehicles and

is detailed in Ref. [29]. X_s is the safe distance in the longitudinal direction and Y_s is that in the lateral direction, which are defined as

$$X_s = X_0 + v_x T_0 + \frac{\Delta v_x^2}{2a_n}, \tag{30}$$

$$Y_s = Y_0 + (v_x \sin\theta + v_{nx} \sin\theta) T_0 + \frac{\Delta v_y^2}{2a_n}, \tag{31}$$

where v_{xn} is the velocity of the nearby vehicle. Δv_x and Δv_y are the longitudinal and lateral approaching velocity, respectively. X_0 is the minimum allowed longitudinal distance and Y_0 is the minimum allowed lateral distance. a_n represents the vehicle acceleration. T_0 is the safe time gap and θ is the heading angle between the two vehicles. Since the potential field increases as the autonomous approach to the nearby vehicle, the autonomous vehicle is preferred to drive along the low potential area and avoid the high potential area, so that the autonomous vehicle can avoid the nearby vehicle in the lane-exchanging scenarios.

Besides the potential field of the nearby vehicle, the potential field of the road boundary is defined to prevent the vehicle from leaving the lane. The potential field of the road boundary is written as

$$U_R(X,Y) = \begin{cases} a_R(SD_R(X,Y) - D_a)^2 & SD_R(X,Y) < D_a, \\ 0 & SD_R(X,Y) > D_a, \end{cases} \tag{32}$$

where $SD_R(\bullet)$ is the singed distance between the autonomous vehicle and the road boundary. D_a is the safety distance from the lane boundary. a_R is the intensity parameter. With the potential field defined for the lane boundary, the autonomous vehicle is prevented from leaving the lane.

The functions of the potential fields are nonlinear and nonconvex, so as the problem of controller design. Its solution is thus time-consuming and computationally expensive. In order to reduce the computational cost, the potential fields are approximated by convex functions via coordinate transformation. The controller design problem can thus be converted into a convex quadratic optimization problem. The convex processes are detailed in Ref. [30] and thus omitted here.

3.3 Cost Function and Constraints

The control objective is to avoid the nearby vehicle while performing the lane-change maneuver at the same time. The lateral and longitudinal motion of the autonomous vehicle have to be manipulated simultaneously. As the autonomous will change to the adjacent lane where the nearby vehicle drives, the desired trajectory is set as the centerline of the adjacent lane. Therefore, the cost function considering the nearby vehicle, the road boundaries, and the trajectory tracking errors is written as

$$J = \sum_{k=1}^{N} (U_o(t+k|t) + U_R(t+k|t)) + \sum_{k=0}^{N-1} \left\| u_c(t+k|t) \right\|_{\boldsymbol{R}} + \sum_{k=1}^{N} \left\| \eta(t+k|t) - \eta_{des}(t+k|t) \right\|_{\boldsymbol{Q}}, \tag{33}$$

where $U_0(t+k|t)$ is the potential fields of the nearby vehicle of time step $(t+k)$ which is computed at time step t, similar to the potential filed of the road boundary $U_R(t+k|t)$. The control effort is $u_c(t+k|t)$ and its corresponding weighting matrix is $\boldsymbol{R}$. $\eta_{des}(t+k|t)$ is the desired system outputs that contains the lateral position and the yaw angle of the centerline of the target lane, as well as the desired velocity. $\boldsymbol{Q}$ is the weighting matrix of the trajectory tracking error.

After defining the cost function, the control efforts can be computed by solving the receding horizon optimization problem. The vehicle system model and the control saturation are considered as the constraints of the optimization problem. Meanwhile, the vehicle states needs to be confined in the reasonable ranges to ensure driving safety and ride comfort. Then, the optimization problem can be expressed as

$$\begin{aligned} &\min_{\boldsymbol{u}(t+k|t),\ldots,\boldsymbol{u}(t+k+N-1|t)} J(\boldsymbol{\xi}(t+k|t), \boldsymbol{u}(t+k|t)), \\ &s.t.\ \boldsymbol{\xi}(t+k+1|t) = \boldsymbol{A_k}\boldsymbol{\xi}(t+k|t) + \boldsymbol{B_k}\boldsymbol{u}_c(t+k|t), \\ &\boldsymbol{\eta}(t+k|t) = \boldsymbol{C_k}\boldsymbol{\xi}(t+k|t), \\ &\boldsymbol{u}_{c\min} < \boldsymbol{u}_c(t+k|t) < \boldsymbol{u}_{c\max}, \\ &\Delta\boldsymbol{u}_{c\min} < \Delta\boldsymbol{u}(t+k|t) < \Delta\boldsymbol{u}_{c\max}, \\ &\boldsymbol{u}(t+k+1|t) = \boldsymbol{u}(t+k|t) + \Delta\boldsymbol{u}(t+k|t), \\ &\text{for } k = 0, 2, 3, \ldots, N-1, \end{aligned} \tag{34}$$

where $\boldsymbol{u}(t+k|t)$ represents the control effort of the time step $(t+k)$ computed at time step t. The $\boldsymbol{u}_{c\min}$ and $\boldsymbol{u}_{c\max}$ are the lower bound and the upper bound of the control effort. Considering the actuator saturation, the minimum and maximum steering angle are $\delta_{\min}$ and $\delta_{\max}$, the minimum and maximum driving torque are $T_{\min}$ and $T_{\max}$. Then the constraints of the control efforts are

$$\boldsymbol{u}_{c\min} = \begin{bmatrix} \delta_{\min} & T_{\min} \end{bmatrix}^{\mathrm{T}}, \boldsymbol{u}_{c\max} = \begin{bmatrix} \delta_{\max} & T_{\max} \end{bmatrix}^{\mathrm{T}}. \tag{35}$$

Similarly, the constraints of the incremental of the control efforts are considered. The $\Delta \boldsymbol{u}(t+k|t)$ is confined by its lower bound $\Delta \boldsymbol{u}_{c\min}$ and its upper bound $\Delta \boldsymbol{u}_{c\max}$. Define the minimum and maximum steering angle between two steps as $\Delta\delta_{\min}$ and $\Delta\delta_{\max}$, and the minimum and maximum driving torque between two steps as $\Delta T_{\min}$ and $\Delta T_{\max}$. Then the constraints of $\Delta \boldsymbol{u}(t+k|t)$ are bounded as

$$\begin{cases} \Delta \boldsymbol{u}_{c\,\min} = \left[\ \Delta\delta_{\min}\ \ \Delta T_{\min}\ \right]^{\mathrm{T}}, \\ \Delta \boldsymbol{u}_{c\,\max} = \left[\ \Delta\delta_{\max}\ \ \Delta T_{\max}\ \right]^{\mathrm{T}}. \end{cases} \tag{36}$$

Under the MPC scheme, a sequence of control efforts are computed, whereas only the first one is sent to drive the autonomous vehicle. More details about the MPC algorithm can be found in Ref. [31].

4 Driving Data and Simulation Validation

The on-road driving data from the Highway Drone Dataset is used to verify the trajectory prediction method. The proposed method is used to anticipate the trajectory of the nearby vehicle. Based on the predicted trajectory, the potential-field-based MPC approach is then utilized to conduct the lane-exchanging maneuver and avoid possible collisions. The designed control method is validated through simulation studies.

4.1 Trajectory Prediction Results

The developed vehicle trajectory prediction method is verified through the Highway Drone Dataset that contains naturalistic vehicle trajectories recorded on German Highway [32]. In the lead-lag driving condition studied in this paper, the effect of the autonomous vehicle on the nearby vehicle is assumed to be small. The vehicle trajectory, including vehicle type, size and maneuver, is collected using a drone from the aerial perspective. The vehicle positions are extracted via the state-of-the-art computer vision algorithms. By learning the on-road driving data, the vehicle trajectory can be anticipated by the proposed method.

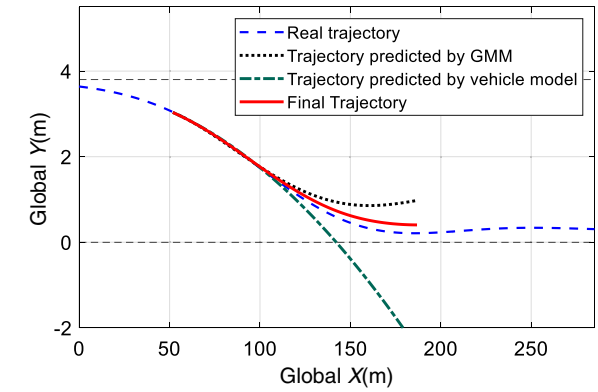

Figure 6 Trajectory prediction at 1.4 s after the start of lane change

The vehicle trajectory is predicted at different time instance after the start of lane change. Since the nearby vehicle changes to the adjacent lane in the lane-exchanging scenario, the start of lane-change is defined as the instance when the vehicle position is around the centerline of its original lane. The historical trajectory is used to predict the future trajectory for 4 s ahead. The trajectory prediction results at the time instance 0.4 s, 1.4 s, and 2.4 s after the start of lane-change are shown in Figures 5–7.

Figure 5 shows the vehicle trajectory that is predicted at 0.4 s after the start of lane-change. The trajectory prediction is accurate at the beginning of the prediction. The prediction error increases with the prediction time and reaches to 0.2 at the longitudinal position 150 m. The final trajectory has smaller errors than the trajectories predicted either by the GMM method or the vehicle mode.

In Figure 6, the vehicle trajectory is predicted at 1.4 s after the start of lane-change. By combing the GMM

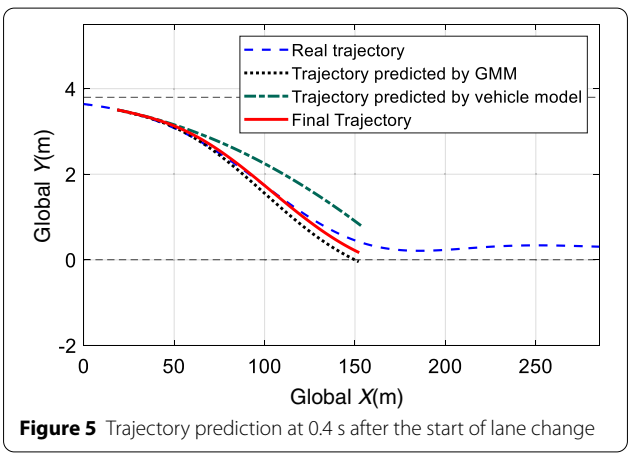

Figure 5 Trajectory prediction at 0.4 s after the start of lane change

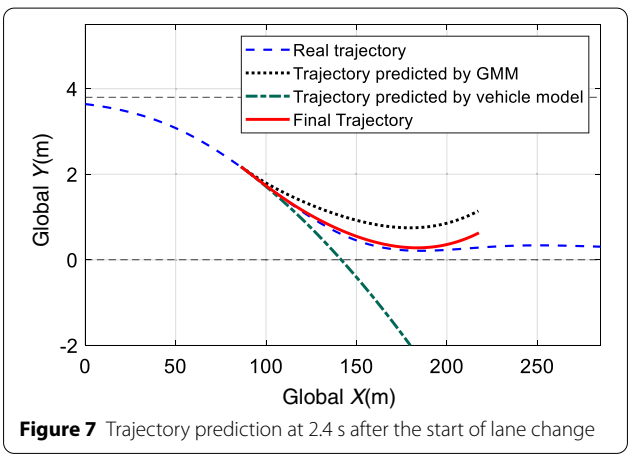

Figure 7 Trajectory prediction at 2.4 s after the start of lane change

method and the vehicle model, the prediction error of the final trajectory can be reduced.

Similarly, the trajectory predicted at 2.4 s after the start of lane-change is depicted in Figure 7. The trajectory prediction by the vehicle model is accurate in the short-term, whereas the trajectory predicted by the GMM method performs better in the long-term. The final trajectory takes advantage of the two prediction methods such that it matches the real trajectory with small prediction errors.

By applying the proposed method, the nearby vehicle trajectory can be predicted with small prediction errors. The predicted trajectory is utilized in the potential-field-based MPC approach for the motion control of the autonomous vehicle, which will be detailed in the next subsection.

4.2 Lane-exchanging Control Performance

Based on the predicted trajectory, the autonomous vehicle can cooperate with the nearby vehicle in the lane-exchanging scenarios. The potential fields are constructed along the predicted trajectory of the nearby vehicle. Then, the potential-field-based MPC is developed for the motion control of the autonomous vehicle to avoid possible collisions while changing to the adjacent lane. A full-vehicle model is built in CarSim® software and the vehicle parameters can be found in Ref. [16]. The nearby vehicle velocity is obtained from trajectory prediction as 32 m/s, meanwhile, the desired velocity of the autonomous vehicle velocity is set as 28 m/s in the lane-exchanging scenario.

Since the initial longitudinal distances between the two vehicles are varying in real driving conditions, the situations of different initial longitudinal distances are studied. When the initial longitudinal distance is 10 m, the trajectories of the two vehicles are shown in Figure 8. The vehicle trajectories when the initial longitudinal distance is 30 m can be found in Figure 9.

As shown in Figures 8 and 9, the autonomous vehicle changes to the adjacent lane by applying the proposed driving strategy. Although the initial longitudinal distances are different, the autonomous vehicle can avoid the nearby vehicle in the lane-exchanging scenario. The relative longitudinal distance increases with the traveling time to ensure driving safety. The driving trajectories of the autonomous vehicle are different when the initial longitudinal distances are 10 and 30 m. When the initial longitudinal distance is 10 m, the autonomous vehicle turns to the right-side to avoid the nearby vehicle at longitudinal position 30 m. Then, the autonomous vehicle turns to the left-side at longitudinal position 80 m and reaches lateral position 2 m at the longitudinal position 100 m. If the initial longitudinal distance is 30 m, the autonomous vehicle directly changes to the target lane. Its lateral position reaches 2 m at the longitudinal position 50 m and reaches the centerline of the target lane at the longitudinal position 125 m. The effects of the nearby vehicle on the autonomous vehicle decreases, as the relative longitudinal distance increases. Therefore, the autonomous vehicle switches to the adjacent lane at the earlier longitudinal position.

To further illustrate the relative positions of the two vehicles in the lane-exchanging scenario, the vehicle positions at the trajectory crossing point are plotted in Figures 10 and 11.

In Figures 10 and 11, the relative distances between the autonomous vehicle and the nearby vehicle are large enough to prevent possible collisions. When the initial longitudinal distance is 10 m, the trajectories of the two vehicles cross around 4.9 s at the longitudinal position 125 m. The longitudinal distance between the two vehicles is around 40 m as shown in Figure 10. As to the

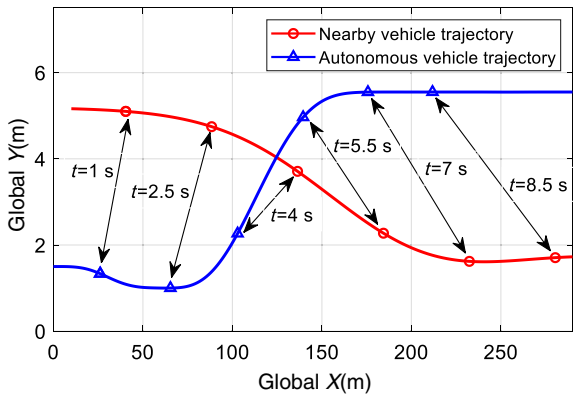

Figure 8 Vehicle trajectories in the lane-exchanging scenario when initial longitudinal distance is 10 m

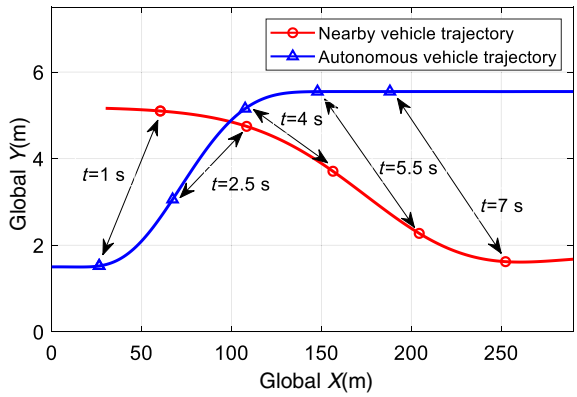

Figure 9 Vehicle trajectories in the lane-exchanging scenario when initial longitudinal distance is 30 m

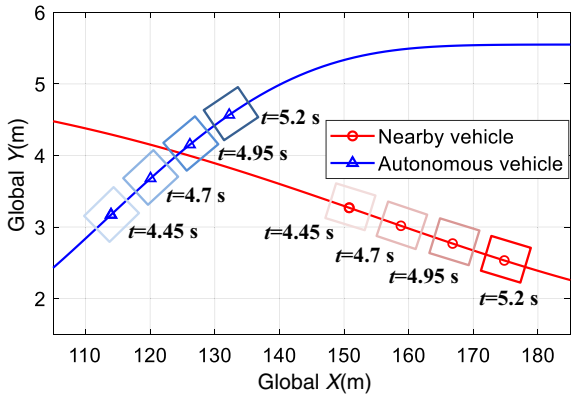

Figure 10 Vehicle positions at the trajectory crossing point when initial longitudinal distance is 10 m

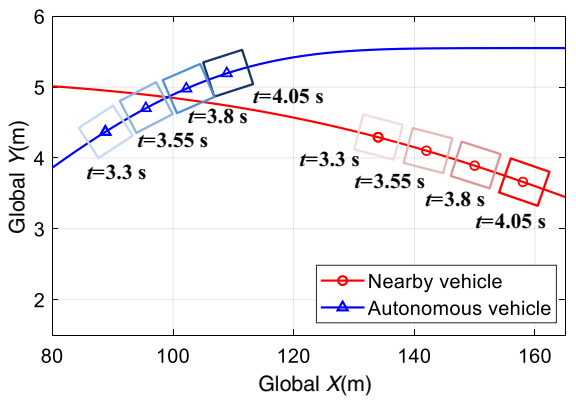

Figure 11 Vehicle positions at the trajectory crossing point when initial longitudinal distance is 10 m

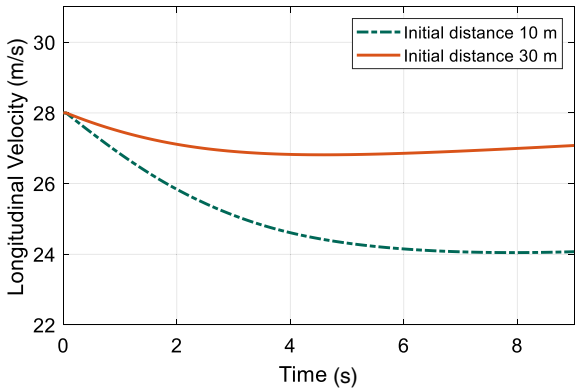

Figure 12 Longitudinal velocity of autonomous vehicle

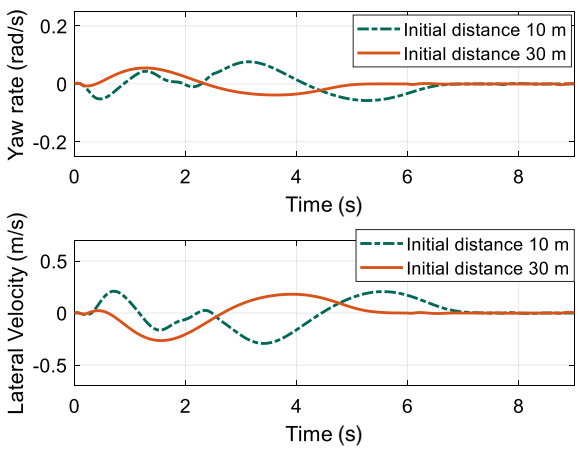

Figure 13 Yaw rate and lateral velocity of autonomous vehicle

driving situation when the initial longitudinal distance is 30 m, the trajectories of the two vehicles cross around 3.7 s at the longitudinal position 100 m. The longitudinal distance between the two vehicles at the cross point is 45 m, as shown in Figure 11. The vehicle positions indicate that the autonomous vehicle passes the trajectory crossing point after the nearby vehicle leaves, which means the autonomous vehicle can avoid the nearby vehicle by applying the proposed driving strategy.

The autonomous vehicle decelerates to avoid the nearby vehicle in the lane-exchanging scenario. The velocity of the autonomous vehicle in the situations of different initial longitudinal distances are illustrated in Figure 12.

Figure 12 shows the longitudinal velocity of the autonomous vehicle decreases to avoid the nearby vehicle under different initial conditions. When the initial longitudinal distance is 30 m, the autonomous vehicle slightly reduces to 27 m/s at 4 s and then increases. If the initial longitudinal distance is 10 m, the autonomous vehicle velocity decreases from 28 m/s to 26 m/s. Due to the smaller initial longitudinal distance, the effects of the nearby vehicle on the autonomous vehicle is larger. Therefore, the autonomous vehicle applies larger deceleration in the driving situation when the initial longitudinal distance is 10 m.

The lateral velocity and yaw rate of the autonomous vehicle in the lane-exchanging scenario are depicted in Figure 13.

In Figure 13, the yaw rate and lateral velocity of the autonomous vehicle can converge by applying the proposed driving strategy. When the initial longitudinal distance is 30 m, the yaw rate increases to 0.05 rad/s and decreases to −0.05 rad/s, and the lateral velocity decreases to −0.25 m/s and increases to 0.2 m/s in the lane-exchanging scenario. Both the yaw rate and lateral velocity converge at 6 s when the autonomous vehicle reaches the target lane. If the initial distance is 10 m, the autonomous vehicle needs more time to reach the target lane. Its yaw rate and lateral velocity have more oscillations and take more time to settle at 7 s.

The driving data validation and simulation results show that the autonomous vehicle can avoid the nearby vehicle in the lane-exchanging scenario by applying the proposed driving strategy.

5 Conclusions

This paper proposes a lane-exchanging driving strategy by combining the trajectory prediction of the nearby vehicle and the motion control of the autonomous vehicle. The trajectory of the nearby vehicle is predicted by the GMM method and the vehicle kinematic model. The lane-exchange maneuver is performed to cooperate with the nearby vehicle using the potential-field-based MPC approach. The proposed driving strategy is validated through the on-road driving data and the simulations. The results show that the autonomous vehicle can avoid the nearby vehicle in the lane-exchanging scenarios. This study considers only one nearby vehicle for simplicity. In the following works, the complex driving situations involving multiple nearby vehicles will be investigated.

Acknowledgements
Not applicable.

Author contributions
YC and HY conceived and proposed the idea of the lane-exchanging driving problem; YC developed the vehicle model and devised the MPC based controller; HY and JZ devised the algorithms of the trajectory prediction; YC prepared the manuscript, HY and DC assisted with the manuscript revision. All authors read and approved the final manuscript.

Authors' information
Yimin Chen is with *the School of Marine Science and Technology, Northwestern Polytechnical University, Xi'an, China*. He received his B.S. degrees in *Mechanical Design from Central South University, Hunan, China*, in 2012, and his M.S. degrees in *Mechanical Engineering from Xi'an Jiaotong University, Xi'an, China* in 2015. He obtained his Ph.D. degrees in *the Walker Department of Mechanical Engineering at the University of Texas at Austin, Austin, TX, USA*, in 2019. He was a Postdoctoral Fellow at *the Department of Mechanical and Mechatronics Engineering, University of Waterloo, Waterloo, Canada*, in 2020. His research interests include automated vehicles, vehicle dynamics and control, and personalized vehicle control systems.
Huilong Yu received his M.Sc. degree in mechanical engineering from *Beijing Institute of Technology*, *China*, and the Ph.D. degree in mechanical engineering from *Politecnico di Milano, Milano, Italy*, in 2013 and 2017, respectively. He was a postdoctoral Research Fellow of advanced vehicle engineering with *the University of Waterloo, Waterloo, CA*. He is now a professor with *the School of Mechanical Engineering* in *Beijing Institute of Technology, Beijing, China*. His research interests include vehicle dynamics, vehicular optimal design and control, and autonomous driving.
Jinwei Zhang received the B.S degree in *Worcester Polytechnic Institute, US*, double major in Robotics Engineering and Electrical & Computer Engineering. He is currently pursuing M.S. degree in *University of Waterloo*, major in Mechanical and Mechatronics Engineering, under the supervision of Prof. Dongpu Cao. His current research focuses on the behavior analysis of lane-changing scenario, and the motion prediction of surrounding scenes applied on autonomous driving.
Dongpu Cao received the Ph.D. degree from *Concordia University, Canada*, in 2008. He is a Professor at Tsinghua University. His current research focuses on driver cognition, automated driving and cognitive autonomous driving. He has contributed more than 200 papers and 3 books. He received the SAE Arch T. Colwell Merit Award in 2012, IEEE VTS 2020 Best Vehicular Electronics Paper Award and 6 Best Paper Awards from international conferences. Prof. Cao has served as Deputy Editor-in-Chief for *IET Intelligent Transport Systems Journal*, and an Associate Editor for *IEEE Transactions on Vehicular Technology*, *IEEE Transactions on Intelligent Transportation Systems*, *IEEE/ASME Transactions on Mechatronics*, *IEEE Transactions on Industrial Electronics*, *IEEE/CAA Journal of Automatica Sinica*, *IEEE Transactions on Computational Social Systems*, and *ASME Journal of Dynamic Systems, Measurement and Control*. Prof. Cao is an IEEE VTS Distinguished Lecturer.

Funding
Supported by Project of National Natural Science Foundation of China (Grand No.52102469), Science and Technology Major Project of Guangxi (Grant Nos. AB21196029 and AA18242033), State Key Laboratory of Automotive Safety and Energy (Grant No. KF2014).

Competing interests
The authors declare that they have no competing interests.

Author Details
[1]School of Marine Science and Technology, Northwestern Polytechnical University, Xi'an 710072, China. [2]School of Mechanical Engineering, Beijing Institute of Technology, Beijing 100081, China. [3]Department of Mechanical and Mechatronics Engineering, University of Waterloo, Waterloo, Canada. [4]School of Vehicle and Mobility, Tsinghua University, Beijing 100084, China.

Received: 4 December 2020 Revised: 6 May 2022 Accepted: 20 May 2022
Published online: 11 June 2022

References

[1] D González, J Pérez, V Milanés, et al. A review of motion planning techniques for automated vehicles. *IEEE Trans. Intelligent Transportation Systems*, 2016, 17(4): 1135-1145.
[2] P Koopman, M Wagner. Autonomous vehicle safety: An interdisciplinary challenge. *IEEE Intelligent Transportation Systems Magazine*, 2017, 9(1): 90-96.
[3] D J Fagnant, K M Kockelman, P Bansal. Operations of shared autonomous vehicle fleet for Austin, Texas, market. *Transportation Research Record*, 2015, 2563(1): 98-106.
[4] N Li, D W Oyler, M Zhang, et al. Game theoretic modeling of driver and vehicle interactions for verification and validation of autonomous vehicle control systems. *IEEE Transactions on Control Systems Technology*, 2017, 26(5): 1782-1797.
[5] Y Chen, J Wang. Trajectory tracking control for autonomous vehicles in different cut-in scenarios. *Proceedings of the 2019 American Control Conference*, 2019: 4878-4883.
[6] N Deo, A Rangesh, M M Trivedi. How would surround vehicles move? a unified framework for maneuver classification and motion prediction. *IEEE Transactions on Intelligent Vehicles*, 2018, 3(2): 129-140.
[7] J Wiest, M Hoffken, U Krebel, et al. Probabilistic trajectory prediction with gaussian mixture models. *IEEE Intelligent Vehicles Symposium*, 2012: 141-146.
[8] A Houenou, P Bonnifait, V Cherfaoui, et al. Vehicle trajectory prediction based on motion model and maneuver recognition. *IEEE/RSJ International Conference on Intelligent Robots and Systems*, 2013: 4363-4369.
[9] G Xie, H Gao, L Qian, et al. Vehicle trajectory prediction by integrating physics-and maneuver-based approaches using interactive multiple models. *IEEE Transactions on Industrial Electronics*, 2017, 65(7): 5999-6008.
[10] A Khosroshahi, E Ohn-Bar, M M Trivedi. Surround vehicles trajectory analysis with recurrent neural networks. *In 2016 IEEE 19th International Conference on Intelligent Transportation Systems*, 2016: 2267-2272.
[11] Y Chen, C Hu, J Wang. Motion planning with velocity prediction and composite nonlinear feedback tracking control for lane-change strategy of autonomous vehicles. *IEEE Trans. on Intelligent Vehicles*. 2019, 5(1): 63-74.
[12] Y Xing, C Lv. Dynamic state estimation for the advanced brake system of electric vehicles by using deep recurrent neural networks. *IEEE Transactions on Industrial Electronics*, 2019, 67(11): 9536-9547.
[13] Z Deng, D Chu, C Wu, et al. Curve safe speed model considering driving style based on driver behaviour questionnaire. *Transportation Research Part F: Psychology and Behaviour*, 2019, 65: 536-547.

[14] Li, M, H Cao, X Song, et al. Shared control driver assistance system based on driving intention and situation assessment. *IEEE Transactions on Industrial Informatics*, 2018, 14(11): 4982-4994.
[15] G Li, Y Wang, F Zhu, et al. Drivers' visual scanning behavior at signalized and unsignalized intersections: A naturalistic driving study in China. *Journal of Safety Research*, 2019, 71: 219-229.
[16] Y Chen, X Zhang, J Wang. Robust vehicle driver assistance control for handover scenarios considering driving performances. *IEEE Trans. on Systems, Man and Cybernetics: Systems,* 2019, 51(7): 4160-4170.
[17] Y Chen, C Stout, A Joshi, et al. Driver assistance lateral motion control for in-wheel-motor-driven electric ground vehicles subject to small torque variation. *IEEE Transactions on Vehicular Technology*, 2018, 67(8): 6838-6850.
[18] Y Chen, J Zha, J Wang. An autonomous T-intersection driving strategy considering oncoming vehicles based on connected vehicle technology. *IEEE/ASME Transactions on Mechatronics*, 2019, 24(6): 2779-2790.
[19] Y Chen, C Hu, J Wang. Human-centered tracking control for autonomous vehicle with driver cut-in behavior prediction. *IEEE Trans. on Veh. Technol*, 2019, 68(9): 8461-8471.
[20] C Hu, Z Wang, H Taghavifar, et al. MME-EKF-based path-tracking control of autonomous vehicles considering input saturation. *IEEE Transactions on Vehicular Technology*, 2019, 68(6): 5246-5259.
[21] H Yu, F Castelli-Dezza, F Cheli. Optimal design and control of 4-IWD electric vehicles based on a 14-DOF vehicle model. *IEEE Transactions on Vehicular Technology*, 2018, 67(11): 10457-10469.
[22] H Zhang, W Zhao. Decoupling control of steering and driving system for in-wheel-motor-drive electric vehicle. *Mechanical Systems & Signal Processing*, 2018, 101: 389-404.
[23] H Zhang, W Zhao, J Wang. Fault-tolerant control for electric vehicles with independently driven in-wheel-motors considering individual driver steering characteristics. *IEEE Transactions on Vehicular Technology*, 2019, 68(5):4527-4536.
[24] J Wang, J Wang, R Wang, et al. A framework of vehicle trajectory replanning in lane exchanging with considerations of driver characteristics. *IEEE Transactions on Vehicular Technology*, 2016, 66(5): 3583-3596.
[25] M Ganslerer, R F Hartl. Collaborative vehicle routing: a survey. *European Journal of Operational Research*, 2018, 268(1): 1-12.
[26] A Doshi, M M Trivedi. Tactical driver behavior prediction and intent inference: A review. *In 2011 14th International IEEE Conference on Intelligent Transportation Systems*, 2011: 1892-1897.
[27] Y Chen, Y C Lu, W Chu. A cooperative driving strategy based on velocity prediction for connected vehicles with robust path-following control. *IEEE Internet of Things Journal*, 2020, 7(5): 3822-3832.
[28] H Wang, Y Huang, A Khajepour, et al. Crash mitigation in motion planning for autonomous vehicles. *IEEE Transactions on Intelligent Transportation Systems*, 2019, 20(9): 3313-3323.
[29] J Schulman, J Ho, A X Lee. Finding locally optimal, collision-free trajectories with sequential convex optimization. *Robotics: Science and Systems*, 2013, 9(1): 1-10.
[30] Y Rasekhipour, A Khajepour, S K Chen, et al. A potential field-based model predictive path-planning controller for autonomous road vehicles. *IEEE Transactions on Intelligent Transportation Systems*, 2016, 18(5):1255-1267.
[31] Y Chen, J Wang. In-wheel-motor-driven electric vehicles motion control methods considering motor thermal protection. *ASME Trans. J. Dyn. Syst. Meas. Control*, 2019, 141(1): 11-15.
[32] R Krajewski, J Bock, L Kloeker, et al. The highd dataset: A drone dataset of naturalistic vehicle trajectories on german highways for validation of highly automated driving systems. *In 2018 21st International Conference on Intelligent Transportation Systems*, 2018: 2118-2125.

Submit your manuscript to a SpringerOpen journal and benefit from:

► Convenient online submission
► Rigorous peer review
► Open access: articles freely available online
► High visibility within the field
► Retaining the copyright to your article

Submit your next manuscript at ► springeropen.com